Experimental and numerical simulation of a two-dimensional unglazed transpired solar air collector

Messaoud BADACHE[1*], Daniel R. ROUSSE[2], Stéphane HALLÉ[3], Guillermo QUESADA[4]

Technologies of energy and energy efficiency industrial research chair (t3e), Department of mechanical engineering, École de technologie supérieure, Université du Québec
1100, Notre-Dame St. West, Montreal, H3C 1K3, Canada

[1*] **Corresponding author:** messaoud.badache.1@ens.etsmtl.ca

[2]daniel.rousse@etsmtl.ca

[3]stephane.halle@etsmtl.ca

[4]guillermo.quesada@etsmtl.ca

Abstract

In this paper, the thermal efficiency of a solar air collector called unglazed transpired collector (UTC) has been investigated both experimentally and numerically. Experimental investigations were carried out in a laboratory with a controlled environment. Measurements of temperatures, air velocity and irradiance were performed for three air mass flow rates, three distinct irradiances and two plenum thicknesses. Perforations in the form of slot were selected to enable a comparison with 2D numerical simulations. Meanwhile, a commercial finite volume software was used to model the heat transfer and air flow through the collector. The CFD simulation shows good agreement with experimental results. It was found that a weak heat exchange process took place in the plenum: the maximum efficiency difference between the two plenum thicknesses (5 and 15 cm) was only 3.25%.

Keywords: Computational Fluid Dynamics, efficiency, unglazed transpired solar air collector.

Nomenclature:

A_{coll}	collector area (m^2)
A_p	pipe cross section surface area (m^2)
b	slot's thickness (mm)
Cp	specific heat capacity of air (J/kg·K)
g	gravity force (m/s^2)
G_T	absorbed irradiance (W/m^2)
H	absorber plate height (cm)
L	pitch of between slots (mm)
$\dot{m}$	air mass flux ($kg/s/m^2$)
P	mean dynamic pressure (Pa)
Pr_t	turbulent Prandtl number
$\dot{q}$	volumetric heat source term (W/m^3)
T_{amb}	ambient air temperature (^oC)
T_{out}	outlet air temperature (^oC)
$T_{in,h}$	average air temperature at the slot inlet (^oC)
$T_{out,h}$	average air temperature at the slot outlet (^oC)
T_p	average plate temperature (^oC)
v	volume (m^3)
$\overline{V}$	average outlet air velocity (m/s)
w	plenum thickness (cm)
z	height of the air outlet opening (cm)
ΔT	temperature difference (^oC)

Greek symbols

α	absorption coefficient
β	thermal expansion coefficient (1/K)
ε	turbulent dissipation rate (m^2/s^3)
ε_{UTC}	heat exchange effectiveness

ε_f	heat exchange effectiveness in the front region
ε_b	heat exchange effectiveness in the back region
ε_h	heat exchange effectiveness in the slot region
ε_p	thermal emissivity of the absorber plate surface
η	collector efficiency
λ	thermal conductivity (W/m·K)
ρ_{air}	air density (kg/m^3)
δ_{ij}	Kronecker delta
ν	molecular kinematic viscosity (m^2/s)
ν_t	turbulent kinematic viscosity (m^2/s)
S_{ij}	mean-strain tensor
k	kinetic turbulent energy (m^2/s^2)
y^+	non-dimensional distance

1. Introduction

Unglazed transpired collectors (UTC's) are now a well-recognized solar air heater for heating outside air directly (Arulanandam et al., 1999). They are key components in many engineering applications, such as in institutional and residential heating, industrial processes like sewage wastewater treatment, and food processing. They differ from conventional solar air collectors in that their southern wall is replaced by a black perforated sheet that allows the collection of solar irradiation. Typically, they consist of a thin, black aluminum or galvanized steel cladding perforated by tiny holes, mounted onto a southward facing wall. Incident solar energy raises the temperature of the perforated cladding above the ambient temperature. As a consequence, outside air is heated when it is drawn through the perforations by a ventilation fan. The heated air is directed through an air gap located between the building wall and the absorber plate. The heated air is then used to feed fresh air into buildings and other applications.

The progress achieved on UTC's in the last twenty years has been remarkable, since the early studies conducted by Kutscher (1992; 1993; 1994) , passing through the very

extensive experimental and theoretical works by (Van Decker et al., 2001; Fleck et al., 2002; Athienitis et al., 2011; Badache Messaoud et al., 2012), and on numerical studies presented by (Dymond, Kutscher, 1997; Arulanandam et al., 1999; Gunnewiek et al., 2002; Gawlik et al., 2005; Belusko et al., 2008). All of the aforementioned studies have had similar objectives, principally the development of methods that could be used to estimate the collector's thermal performance (Weerakoon et al., 2004). They have showed that UTC's require good radiative, geometry and air flow rate properties in order to benefit from optimum solar gains with minimum investment cost. A literature review on the works done on UTC's through this period revealed a considerable amount of information published on this subject that cannot be exhaustively reported (Genevès et al., 2012). Thus, the present review will be limited only to numerical works.

2. Literature review

Kutscher (1992) was the first who numerically studied these systems. He used Fluent software with a two-dimensional (2D) numerical model to analyze the influences of several parameters such as hole pitch and diameter, plate thickness, mass flux, and crosswind on the heat transfer on the front surface, in the hole, and on the back surface of a repeating pattern. This pattern was limited to the section of the plate from the hole centerline to the midpoint between hole centerlines. Following Kutscher's work, Cao et al. (1993) performed a 2D numerical study, in which they modeled the flow through long slit-like perforations rather than the more common circular holes. They considered only the heat transfer occurring in the hole and at the front of the plate. The flow was assumed to be transverse to the slits but parallel to the plate. They showed that 20% of the overall heat transfer occurs in the slot. Gunnewiek developed a 3D CFD model, later simplified to a 2D model (Gunnewiek et al., 1996). The air flow through the perforated plate was modeled as a continuous phenomenon rather than as a process occurring through discrete holes. In addition, the approach of Gunnewiek et al.,(1996) included only the plenum region, with a special set of boundary conditions to model the plate and the ambient air. They concluded that the velocity profile in the plenum depends on whether the flow is dominated by buoyancy forces or by the suction pressure created by the fan. This study was extended later in (Gunnewiek et al., 2002) by taking into account the effect of wind

speed. The results show that wind speed raises the minimum suction velocity needed to prevent flow reversal. Arulanandam et al. (1999) studied the heat transfer effectiveness (ε_{HX}) of the UTC using a commercial CFD software (TASCflow) under no wind conditions. Simulations were carried out over a 3D model of a quarter of a hole for a square pitch. In this study, the authors considered only the heat transfer occurring in the hole and at the front of the plate, the back of the plate was modeled as adiabatic. Simulations were done for various sets of conditions and the results were incorporated into a correlation model for the UTC effectiveness. Gawlik and Kutscher (2002) performed a CFD model on plates with sinusoidal corrugations. The numerical model was used to determine heat loss to the air stream over the corrugated plate as a function of wind speed, suction velocity, and plate geometry. Experimental tests were used in parallel to determine if the numerical model predicted convective heat loss accurately. Assuming a perpendicular and uniform flow, and wind velocity over the plate, they found that flow over the corrugation was ether attached or separated. Correlations for heat loss from the plate to the crosswind were developed for both the attached and separated flow cases.

The effect of the plate conductivity was studied in details by Gawlik et al. (2005). They performed a numerical and experimental investigation of low-conductivity material used for UTC. This study was motivated by the possibility of using a material other than aluminum for cost savings and for applications that do not need a high conductivity. The study concludes that low-conductivity material can be used in UTC's since material conductivity has a small effect on the thermal performance of these collectors.

The earlier studies mentioned above showed that modeling a full-scale UTC requires some simplifications in order to fit the numerical model within the limits of the computer resources (Gunnewiek et al., 1996). Cao et al. (1993) showed that modeling the flow around even a single hole requires several hours of computer time. Indeed two main approaches were explored, one was to include only the plenum region (Gunnewiek et al., 1996; Gunnewiek et al., 2002), the second approach uses symmetry of the UTC system in which simulations were restricted to the perforations region (Kutscher C F, 1992; Cao S et al., 1993; Arulanandam et al., 1999; Gawlik et al., 2005)

Therefore to the best of our knowledge no detailed numerical studies have yet-been undertaken to determine numerically the thermal performance of the whole collector including the plenum and the perforations. Hence, the purpose of the present investigation is to perform an experimental and numerical simulation of a two-dimensional unglazed transpired collector including the plenum and the perforations regions.

Two excellent reviews on the general topic of solar facades: opaque (Quesada et al., 2012a) and transparent and translucent (Quesada et al., 2012b) have recently been available in the literature.

In this paper, the thermal performances of two UTC prototypes are investigated experimentally and with computational fluid dynamics (CFD). The experimental conditions are used as boundary conditions for the numerical simulations. The heat transfer and air flow through the collector are modeled by finite volume commercial software (Fluent, 2012). This software solves the Reynolds–Average Navier–Stokes (RANS) equations coupled with energy conservation equation and turbulence modeling. The low-Reynolds RNG k–ε turbulence model has been employed to simulate the turbulent cases.

This paper is organized as follows: in the next section, a brief description of the experimental procedure is presented. The physical model is presented in Section 4 in which the numerical method is introduced. Governing conservation equations, spatial discretization, boundary conditions and a grid refinement analysis are also presented and discussed in this section. In Section 5, numerical results are presented, discussed and compared with the experimental data. The paper ends with the conclusions, which are stated in Section 6.

3. Experimental setup and test procedure

3.1 Experimental set-up

For the experimental part, two UTCs prototypes have been built, instrumented and tested in laboratory conditions. These will be designated as "*w*-5" (plenum of 5 cm thickness) and "*w*-15" (plenum of 15 cm thickness). A vertical section of the UTC prototype studied is schematically shown in Figure 1. Each prototype involves, a vertical wooden box, an absorber plate, an air gap (plenum) with thickness *w* bounded by the back wall and the absorber plate. The air leaves the plenum via the top back wall. The sides and the back of the collector are well insulated, while the front face was exposed to lamps irradiation and ambient temperature. Note that the air suction system and the artificial source of radiation are not illustrated in Figure 1.

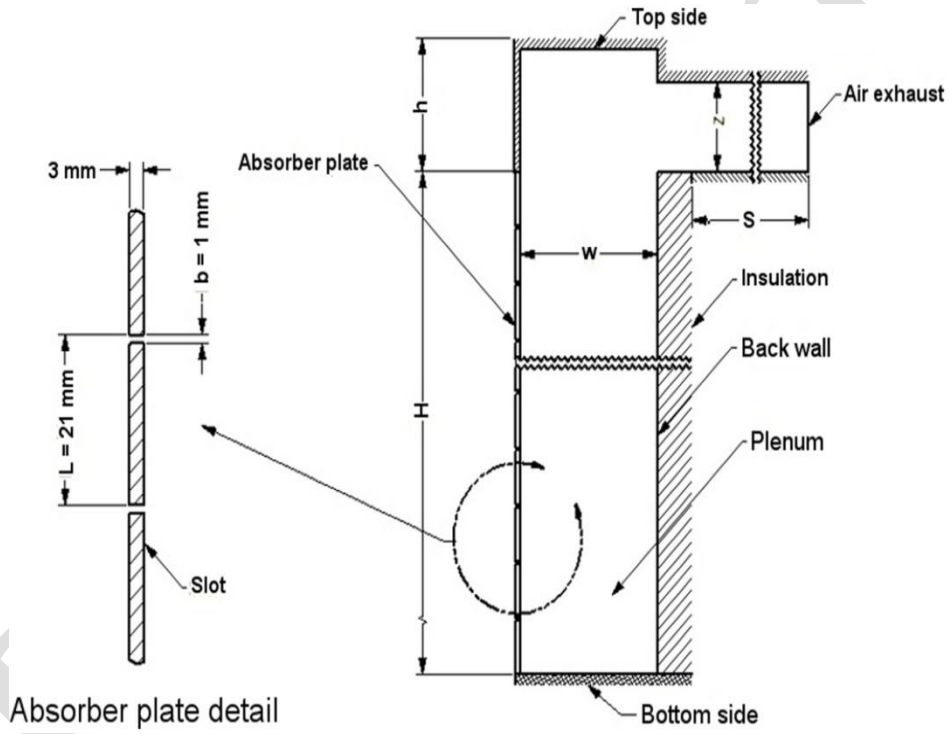

Figure 1: Vertical section of the UTC showing the geometry under investigation

The absorber test plate consists of an aluminum sheet (λ = 202 W/m·K) coated with Thurmalox® 250 selective black coating (ε_p = 0.52) mounted on the front face of the wooden box. The absorber plate has the same dimensions in all tests; 3 mm thick, 48 cm height (*H*) and 36 cm width (not visible in the Figure 1). It includes an equally spaced single row of slots (21 slots), of width *b* = 1 mm, uniformly distributed at a distance *L* = 21 mm, through which air is drawn. This is equivalent to an apparent surface of 0.174 m^2

with about 5% porosity. Laser cuts were used to manufacture these slots with an accuracy of ±0.1 mm.

To test UTC's with two plenums thicknesses, two structural wooden boxes (5 cm and 15 cm thicknesses) were constructed; each box is 32 cm wide by 60 cm of height. The rear part of the box (back plate) consists of 1.9 cm (3/4"), thick plywood, fitted with a rectangular outlet opening fixed at its top center. For each prototype, the absorbed plate was screwed to the wooden box and sealed with a silicone adhesive. Manufacturing imperfections were corrected with spray polyurethane foam. The entire box was insulated with 10 cm thick polystyrene, and reinforced with a layer 0.5 cm thick of thermo-foil, to minimise heat losses and to act as adiabatic walls. The overall thermal resistance is estimated to be equal to 1 m^2K/W. The whole apparatus is positioned on base fixed at the bottom of the collector to ensure its stability.

The air suction system includes the following three parts: an air exhaust pipe; the air suction ventilator; and a variable speed drive. Air is drawn from the plenum by an inline duct ventilator installed in circular pipe line (15 cm OD, 1.5 m length). Mass flow rate and outlet air temperatures are measured upstream of the fan. The air mass flow rate through the collector was controlled by a variable speed drive model (3PN116B, 110/120 V, 60Hz) which allows the adjustment of air mass flux required in the experiments (0.0133, 0.0266, 0.0411 $kg/s/m^2$). Mass flow through the exhaust pipe is measured by a hot wire anemometer (TSI, VELOCICALC Model 9545) with a reading uncertainty of 3% or ±0.015 m/s, whichever is greater. Calculations for air mass flux ($\dot{m}$) have been carried out according to equation $\dot{m} = \rho_{air} \overline{V} A_p / A_{coll}$ where $\overline{V}$ is the average outlet air velocity, which was measured in five positions inside the exhaust pipe line.

Laboratory investigation has required controlled and constant irradiance G_T from an artificial solar simulator that simulates different levels of irradiance. The incident irradiance, both longwave and shortwave, on the plane of the collector is represented by G_T. Tests were performed for 3 levels of irradiance: 300, 450 and 600 W/m^2. The artificial solar simulator involves 28 globe®- projectors with T3/J-TYPE/87 mm, 150 Watts, light bulbs that collectively provide a total radiative intensity of 4.2 kW.

Compared to the solar irradiation, the lamps spectrum is shifted to the infrared. Lamps radiation has to be homogeneous on plane of the collector (absorber plate). Indeed, the lamps were installed in such a way to obtain an irradiance of the test plate within ± 3% uniformity. The uniformity of the incident irradiance was confirmed by use of a Kipp & Zonen CMP 11 pyranometer. This device not only allowed a scanning of different intensities of the lamps on the collector surface, but it has also provided a measurement of the different irradiance levels needed for the experiments.

3.2 Test procedure

For each plenum thicknesses, three irradiance levels and three mass fluxes were studied. In total, 18 test runs were performed. Each test started by adjusting the irradiance level and the mass flow rate. Temperatures (T_{amb} and T_{out}) were recorded once the steady-state conditions were reached. Fifteen calibrated (0.2 mm diameter) k-type thermocouples (with an uncertainty of ±0.3 °C) have been used for the temperature measurements at several points in the test apparatus. These points were located as follow: four equidistant positions along the back wall and four others along the inner surface of the absorber plate and five thermocouples to determine the ambient temperature. The other thermocouples were located behind the collector and three were placed at outlet opening to measure the outlet air temperature. The temperature recording was carried out using a conventional data acquisition system.

Efficiency has been traditionally used as a measure of heat transfer performance for a UTC. UTC's efficiency is estimated from the ratio of the useful heat gain delivered by the collector divided by the incident irradiance on the collector surface and can be determined by the following equation (1):

$$\eta = \frac{\dot{m}_{out} c_p \left(T_{out} - T_{amb}\right)}{G_T A_{coll}} \quad (1)$$

4. Numerical method

4.1 Physical Problem

The numerical models were designed to gather the essential features of the experimental prototype. They include conductive, convective and radiative heat transfer by which the thermal energy is transferred through the UTC. Ideas for the treatment of combined modes of heat transfer were borrowed from the original work of Rousse (1994; 1996). Note that, only radiation heat exchange between the absorber plate and the surroundings is considered in this study. Based on the former studies (Badache M et al., 2010) the radiation heat exchange between the absorber plate and the back wall has been considered negligible. Wind is very likely to affect the systems performance, no wind condition is likely to be a worst case scenario in terms of heat exchange transfer and thus suitable for design purposes (Kutscher C F, 1992).

The flow is assumed to be steady, turbulent and, two-dimensional. Commercial CFD software (Fluent, V12.1.4) was employed to solve the steady-state Reynolds–averaged Navier–Stokes equations (RANS) coupled with the energy conservation. The Boussinesq approximation was used to account for the density variation. Thermophysical properties of the fluid are evaluated at a reference temperature and assumed to be constant, except in the buoyancy term. The third dimension of the collector is considered large enough so that the flow and heat transfer are two-dimensional. Under the above assumptions, the mathematical model is described by the following classical governing equations:

Continuity equation

$$\frac{\partial U_j}{\partial x_j} = 0 \tag{2}$$

Momentum conservation equation

$$\frac{\partial (U_i U_j)}{\partial x_j} = -\frac{1}{\rho}\frac{\partial P}{\partial x_i} + \frac{\partial}{\partial x_j}\left(\nu \frac{\partial U_i}{\partial x_j} - \overline{u_i u_j} \right) - g_i \beta \left(T - T\infty \right) \tag{3}$$

Energy conservation equation

$$\frac{\partial (T U_j)}{\partial x_j} = \frac{\partial}{\partial x_j}\left(\frac{\nu}{\mathrm{Pr}} \frac{\partial T}{\partial x_j} - \overline{T' u_j} \right) \tag{4}$$

The term $g_i\beta(T–T_\infty)$ specifically accounts for the effect of the air density variation with the temperature. Variables x_i and x_j are the Cartesian coordinates in the *i*-direction and *j*-

direction, where U_j and T are respectively the time average velocity and temperature while P is the pressure. Gravitational acceleration components are represented by g_i and β is the thermal expansion coefficient. Finally, the turbulent stress $-\overline{u_i u_j}$ and turbulent heat flux $-\overline{T'u_j}$ are derived from the turbulence closure model defined as:

$$-\overline{u_i u_j} = 2\nu_t S_{ij} - \frac{2}{3}k\delta_{ij}, \text{ and } -\overline{T'u_j} = \frac{\nu_t}{\mathrm{Pr}_t}\frac{\partial T}{\partial x_j} \quad (5)$$

in which δ_{ij} is the Kronecker delta, ν_t and Pr_t the turbulent kinematic viscosity and turbulent Prandtl number, respectively (Pr_t = 0.7). The mean-strain tensor is S_{ij} and k is the kinetic turbulent energy.

4.2 Turbulence modeling

The introduction of time-averaged values makes the number of unknowns in the conservation equations greater than the number of equations. Thus, it is necessary to close the system of equations using a turbulence model. Previous numerical studies on UTC's have demonstrated that a laminar flow assumption is sufficient to model the flow appropriately (Kutscher C F, 1992),(Cao S et al., 1993) , (Arulanandam et al., 1999) and (Gawlik et al., 2005). Others have considered turbulence effects with the k-ε turbulence model (Gunnewiek et al., 1996; Khattab, 2001; Gunnewiek et al., 2002). In this study, a main concern has been brought to accurately model the flow in the near-walls regions, where significant velocity and thermal gradients are expected. The assumption of turbulent flow was justified in two ways. First, the presence of slots changes the flow behavior over the absorber plate, and typically creates turbulent recirculation regions in the plenum. Second, the fluid dynamic models, representative of the air motion inside the plenum, show rather complex behaviors involving both turbulent and laminar flows (Gunnewiek et al., 1996). The flow may be laminar or turbulent, depending on the region and the air flow rate through the collector. Apart from the intrinsic difficulty to define the region of the collector where the flow is laminar or turbulent, it is not possible to apply both laminar and turbulent models in a single computational domain. In this context, the Re–Normalisation Group (RNG) k-ε model derived by Orszag et al. (1993) was applied

since this model is frequently used for indoor air simulations that involve both laminar and turbulent conditions (Fuliotto et al., 2010); (Zhang et al., 2007). For brevity, the transport equations for k and ε will not be presented here; full equation sets and details for this model are available in the software user's manual(Fluent, 2012).

4.3 Mesh design and boundary conditions

To accurately predict the velocity and thermal boundary layer developing in the near-wall regions was one of the challenges of this study. The computational grid must resolve both the upstream and downstream flows around the slots. If the boundary layer in the vicinity of these two regions is not resolved adequately, the underlying physics of the flow will be lost and the simulation will be inaccurate. In order to resolve the thermal and velocity boundary layers, a structured mesh grid was used inside the slot, in the solid region itself, and a region located at $x = \pm 1$ cm from the absorber plate (i.e. 1 cm upstream and 1 cm downstream of the plate). A large number of grid points are placed inside the slots where the temperature and velocity gradients are expected to be significant. A relatively coarse non structured mesh grid was used within the rest of the computational domain. Both plenum cases are discretized with the same meshing strategy. Figure 2, shows the grid topology near a slot. Table 1, shows the characteristics of the three meshes (A, B and C) for each plenum case. The parameters N_a, N_b, N_c and N_d represents the number of nodes at the edges of the smallest repeating pattern as shown in Figure 2, while N_t and C_L represents respectively the total number of nodes and cells within the computational domain.

Figure 3 shows the boundary conditions imposed on the computational domain. As presented on Figure 3, three types of boundary conditions were considered:

- **At walls:** The no-slip boundary condition is imposed on all rigid walls. In all cases, vertical (back wall) and horizontal (bottom, top) walls have been considered adiabatic. At the absorber plate, a heat generation source term is introduced by user-defined functions (UDF) that specify the heat generation rate through it. This UDF modifies the heat generation rate (q_{cell} in W/m^3) for each surface cell of the absorber plate in order to account for the radiative heat exchange between the

absorber plate and the surroundings as in equation (6). Note that the sky temperature was specified to be equal to 305 K.

$$q_{cell} = \left[\ \alpha \cdot G_T - \varepsilon \cdot \sigma \cdot (T_p^4 - T_{sky}^4) \ \right] \frac{A_{cell}}{V_{cell}} \qquad (6)$$

- **At the inlet air section**: The left side of the computational domain (i.e. at the distance x_∞) is bounded by a free air stream inlet with an assumed total pressure of 0 Pa. This condition was chosen to ensure that the flow at the slots entrance is not disturbed. Cao et al. (1993) found that a distance $x_\infty = 2L$ was sufficiently large to ensure that the effectiveness was independent of x_∞. In this study, runs were initially made with $x_\infty = 5L$ but finally, this value was reduced to $x_\infty = 2.5L$ equivalent to 5.2 cm from the absorber plate. All subsequent simulations were made on the basis of this condition. The incoming air temperature was specified to be equal to the ambient temperature T_{amb}.
- **At the outlet air section**: An outlet velocity condition was imposed from the velocities measurements on the UTC prototypes.

Table 1: Grid parameters for the two plenums configuration

		C_L	N_t	N_a	N_b	N_c	N_d
Plenum of 5 cm (*w*-5)	Mesh A-5	100 494	67 125	10	5	15	25
	Mesh B-5	168 699	112 997	15	10	20	30
	Mesh C-5	180 342	126 025	30	20	20	30
Plenum of 15 cm (*w*-15)	Mesh A-15	172 961	103 319	10	5	15	25
	Mesh B-15	282 615	220 351	15	10	20	30
	Mesh C-15	393 026	237 281	30	20	20	30

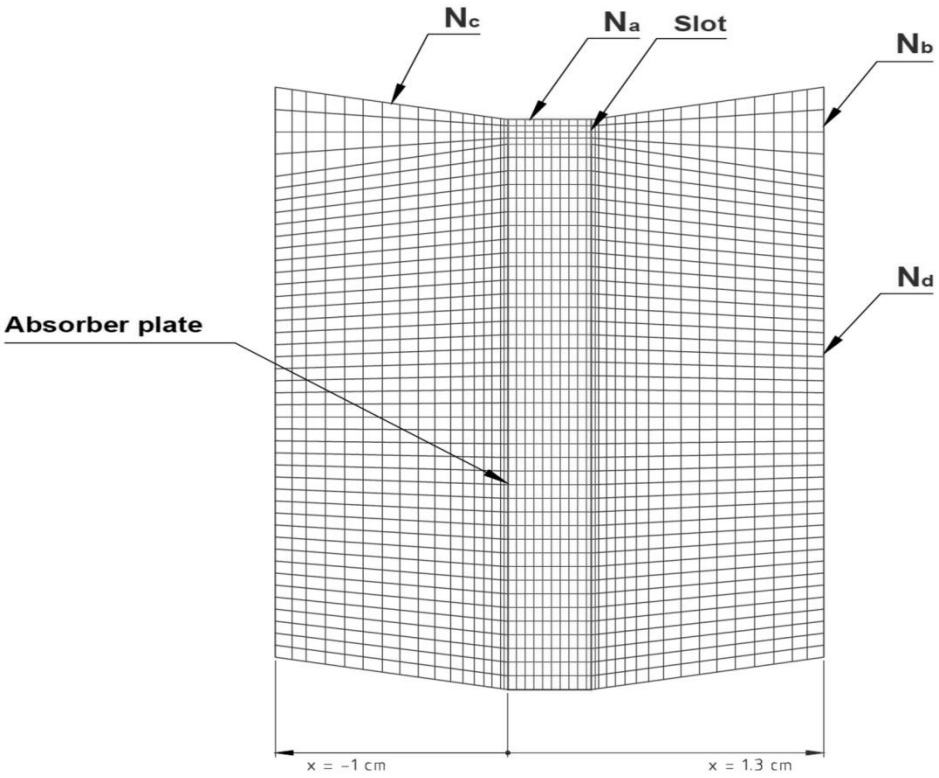

Figure 2: Grid topology near a slot and one spacing L of the plate

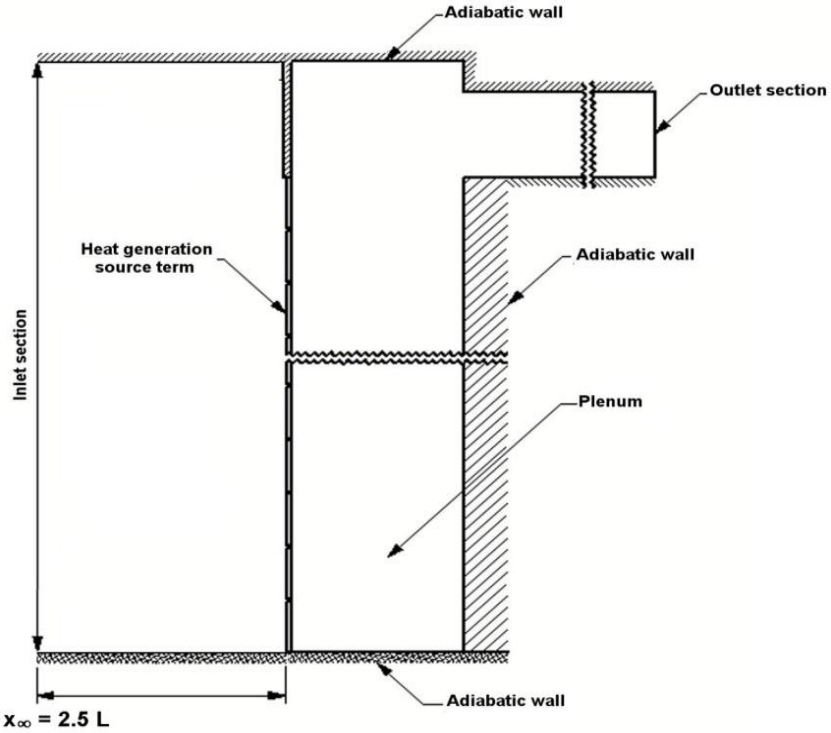

Figure 3: Boundary conditions imposed on the computational domain

4.4 Numerical methodology and grid independence study

The set of governing differential equations (2-4) have been solved numerically via Fluent which is based on a finite volume procedure. Convective and diffusive terms are discretized with a second order upwind scheme. The SIMPLE algorithm of Patankar and Spalding (1972) was used to solve the velocity-pressure coupling. The solution was considered to be converged when the residuals were in the order of 10^{-6} for continuity, momentum, and turbulence quantities and 10^{-10} for energy. All simulations were performed on a i7-960 processor, 3.2 GHz and 12 GB of memory.

A grid independence study was carried out to ascertain the accuracy of the numerical results and to decide what grid size should be used for all the simulations. The efficiency of the UTC was the relevant parameter to be analyzed. The simulation case involving a mass flux of 0.0411 kg/s·m^2 and an irradiance of 600 W/m^2 was considered in the grid independence study. The reason is that this case is the most restrictive in terms of convergence rate. It is noted, that the grid independence study calculation were carried out without account for radiation heat exchanges.

Tables 2 and 3 presents the UTC efficiency and the corresponding y^+ values evaluated at the slots region for the meshes tested and the plenums of 5 cm and 15 cm, respectively. As seen in Table 2, the meshes A-5 and B-5 produce slightly different results than mesh C-5 and the maximum y^+ value are larger than 1. The same is observed for mesh (A-15) and (B-15) (Table 3). To satisfy the condition ($y^+ \leq 1$) required for low Reynolds models, the mesh grid (B-5) and (B-15) were refined. Once, the condition of $y^+ \leq 1$ is fulfilled (within the adapted mesh grid (C-5) and (C-15)) the models were found sufficiently adequate for an estimation of the numerical error. This numerical error, estimated by a mesh refinement analysis, is also known as the discretization error.

The Grid Convergence Index (GCI) method, which is based on the classical Richardson extrapolation (Celik et al., 2008) was used to determine the discretization error. The corresponding computed values of efficiency used in the GCI study are also reported in Table 2 and 3. The numerical uncertainty of the fine-grid solution for the cases (*w*-5) and (*w*-15) are 0.37% and 0.84%, respectively, and the extrapolated values for the efficiency

are 87.27% and 86.07%. From a viewpoint of grid independence of converged solutions, the difference between the extrapolated and fine mesh solution is negligible. The Richardson extrapolated solution for each plenum case cannot be differentiated from the fine grid solution. Consequently, the results presented in the subsequent simulations were calculated using mesh grid (C-5) for plenum (w-5) and (C-15) for plenum (w-15) for which details are provided in Table 1.

Table 2: Efficiency and *y*+ values (plenum of 5 cm)

Mesh	A-5	B-5	C-5	Richardson extrapolation
η (%)	90.08	87.89	87.52	87.27
y+	2.4	2.0	0.5	-
GCI (%)	0.37			

Table 3: Efficiency and *y*+ values (plenum of 15 cm)

Mesh	A-15	B-15	C-15	Richardson extrapolation
η (%)	91.32	87.47	86.64	86.07
y+	2.4	1.5	0.8	-
GCI (%)	0.84			

5. Results

5.1 Comparison with experimental results

The numerical results are presented in this section in terms of the collector efficiency and are compared to experimental data. Results obtained for three air mass fluxes (0.0133, 0.0266 and 0.0411 kg/s·m^2), three irradiance levels (300, 450 and 600 W/m^2) and two plenum thicknesses (5 and 15 cm) are presented.

The experimental measurements are affected by uncertainty, regardless of the quality of instrumentation used and talent of the experimenter. Thus, a correct validation of any measurement used as validation test data, requires a careful check of its quality and accuracy. The classical method of Kline and McClintock (1953) and (Robert J, 1988) has been applied in order to estimate the uncertainty associated with the efficiency measurement. Data related to the instrumentation used in this study stated that the measurement of flow velocity and irradiance have an uncertainty of ±3% and ±1%, respectively. The uncertainty of the temperature measurements is ±0.3 °C. The maximum value for the uncertainty on the efficiency results is thus ±5.4%.

The comparison between CFD simulations and the experimental efficiency measurements for the two plenum thicknesses and three irradiance levels are illustrated in Figures 4, 5 and 6, respectively. Each figure presents the evolution of the efficiency with the mass flux for a given irradiance level. Globally, numerical results show that the predicted efficiency was within the uncertainty range for most of the measured efficiency. For the two plenum cases a good degree of similarity was found at medium and high mass fluxes (0.0266 and 0.0411 kg/s·m^2). However, for a low mass flux, the numerical model over predicts the experimental results. While a slight difference was obtained for low and medium irradiance levels (300 and 450 W/m^2), a significant difference is obtained at high irradiance level (G_T = 600 W/m^2), which was estimated to about 6.8% for plenum (*w*-5) and 13% for plenum (*w*-15) (Figure 6).

On one hand, this disagreement is most likely due to the fact that the sky temperature cannot be known accurately. Whatever the width of the plenum, the collector temperature is at its maximum for the case of G_T = 600 W/m^2 and $\dot{m}$ = 0.0133 kg/s/m^2. Radiative heat losses are important and a slight over estimation of T_{sky} involves a significant underestimation of these radiative losses. When the suction air flow increases, the collector temperature decreases and radiation losses are less significant. On the other hand, factors such as temperature variations in the laboratory (estimated at +/- 1.5°C) and air movement caused by the ventilation system partly explain the differences between the numerical and experimental results. In addition, the horizontal aspect ratio (width/ height)

of our prototype is rather small. Three dimensional flow conditions exist at the vertical edges which cannot be considered in the 2D numerical model.

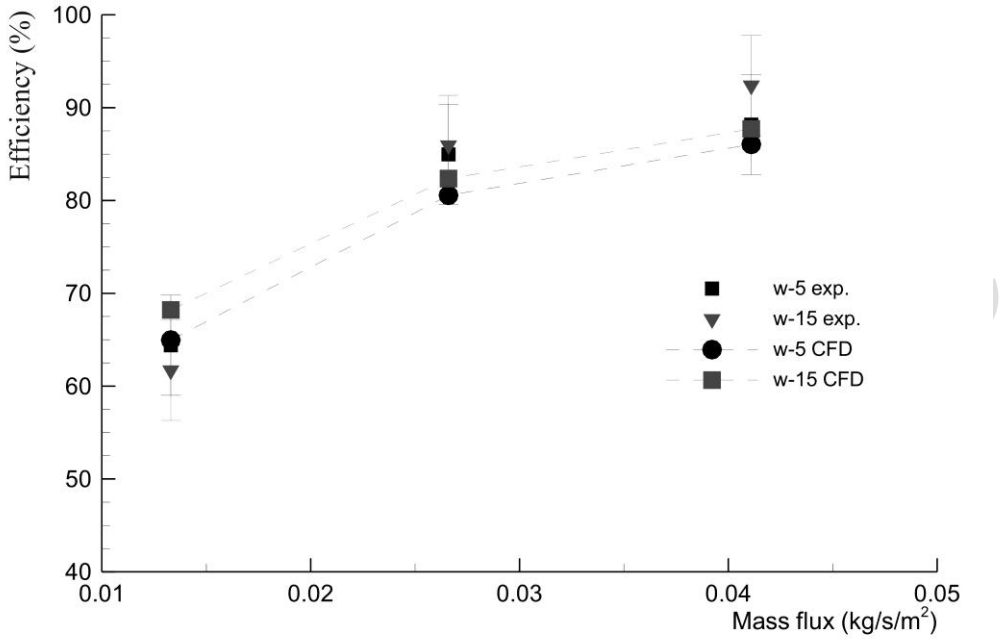

Figure 4: Comparison of the computed and measured efficiency for three air mass fluxes (G_T = 300 W/m^2)

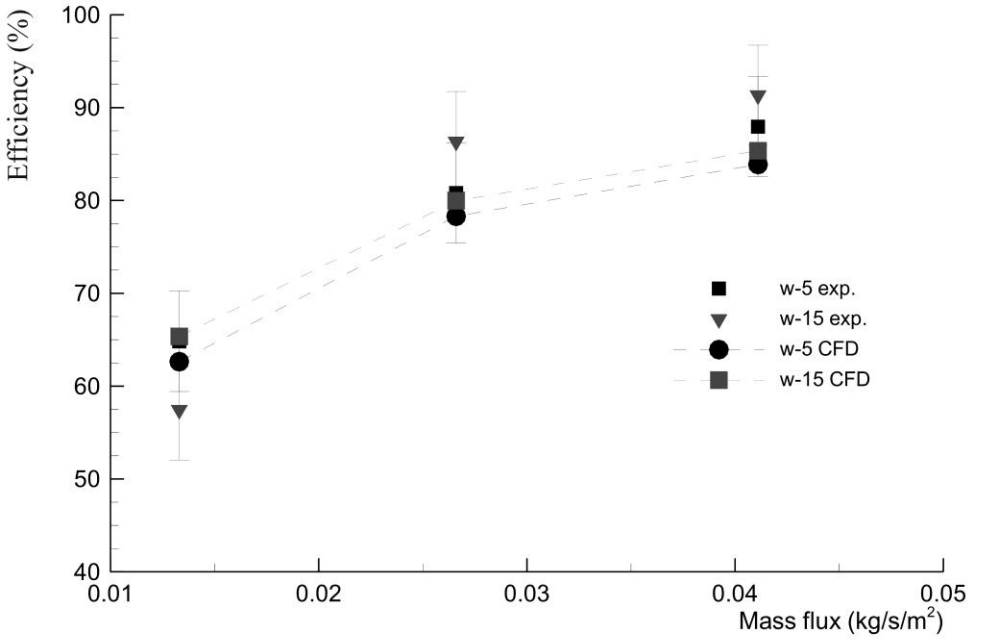

Figure 5: Comparison of the computed and measured efficiency for three air mass fluxes (G_T = 450 W/m^2)

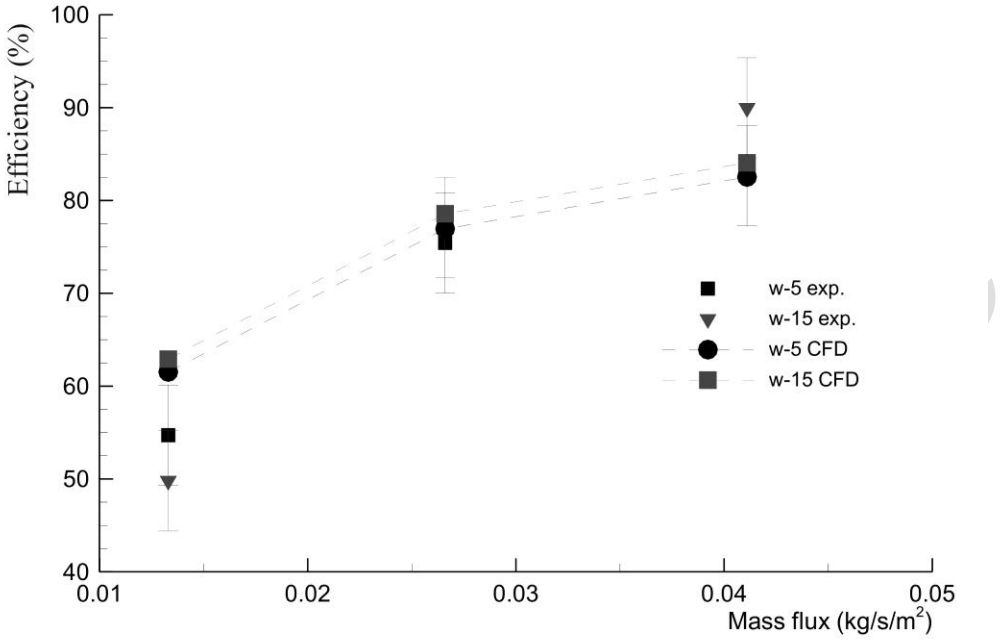

Figure 6: Comparison of the computed and measured efficiency for three air mass fluxes (G_T = 600 W/m^2)

5.2 Effect of mass fluxes

One of the parameters that was used to control the thermal performance of the UTC is the mass flux through the collector, defined as the mass flow rate per unit collector area. It can be found from Figures 4, 5, and 6 that the efficiency increases with increasing air mass fluxes. A high mass flux induces higher velocities through the slots increasing the heat transfer coefficient between the plate and the air.

The computed efficiency is found to rise, rapidly at low mass flux, (by about 16% between 0.0113 and 0.0266 kg/s/m^2), but only slightly (about 5%) at mass flux above 0.0266 kg/s/m^2. These trends are consistent with the results reported by (Kutscher C. F. et al., 1993)) and (Leon, Kumar, 2007)) which have noted a nearly constant efficiency for suction velocities greater than 0.04 and 0.05 m/s. These velocities expressed in terms of mass flow rate per unit area correspond to 0.034 and 0.042 kg/s/m^2. For each irradiance,

there appears to be a mass flux beyond which the heat transfer between the UTC and the flow remains constant.

5.3 Effect of irradiance

For both plenum widths and fixed mass flux, Figures 4, 5 and 6 indicate a small decrease in efficiency (3.5 to 5%) as the irradiance intensity increases from 300 to 600 W/m^2. This decrease is more pronounced at low mass fluxes. Here again, this is explained by high absorber surface temperatures at higher irradiance levels induced by the low capacity of sucked air at moderate mass fluxes to extract all available collector thermal energy. As previously discussed, this increases the heat losses from the absorber plate to the surroundings and, results in a decrease of thermal efficiency. Hence to minimize heat losses from the UTC and to maximize collector efficiency, it is necessary to operate the collector at medium or high mass fluxes especially for high irradiation conditions.

5.4 Effect of plenum thickness

Computed and experimental results show that the efficiency is slightly influenced by the plenum thickness. The larger plenum (*w*-15) gives the higher efficiency. The efficiency between each plenum thickness varied from 1.38 to 3.25%. These slight differences agree with studies done by (Biona M et al., 2002), which showed that for thicknesses between 5 cm to 13 cm, heat exchange effectiveness decreases with plenum thickness, which results in an increase of the efficiency.

The heat exchange effectiveness of the UTC can be defined as the air temperature rise in the collector to the maximum temperature rise (Leon and Kumar, 2007).

$$\varepsilon_{UTC} = \frac{T_{out} - T_{amb}}{T_p - T_{amb}} \tag{7}$$

As mentioned before, the effect of plenum thickness on the efficiency is low compared to the effects of mass flux and irradiance. In a UTC, all the heat exchange process took place at the absorber plate. The fluid motion and heat transfer at the outward face of the absorber is the same regardless the plenum thickness. The same observation is valid for the heat transfer that occur in the slot where the air flow is unaffected by the plenum

thickness. Therefore, the efficiency variation observed between the two plenum cases can only be due to the heat transfer from the back side of the absorber plate to the air.

In order to compare the temperature rise in the slots, the front and back side of the UTC, heat exchange effectiveness can be splited into three partials effectiveness associated with each region such as.

$$\varepsilon_f = \frac{T_{in,h} - T_{amb}}{T_p - T_{amb}} \qquad \varepsilon_h = \frac{T_{out,h} - T_{in,h}}{T_p - T_{amb}} \qquad \varepsilon_b = \frac{T_{out} - T_{out,h}}{T_p - T_{amb}} \tag{8}$$

Where $T_{ih,h}$ and $T_{out,\,h}$ represent the average air temperature at the slot entrance and exit, respectively. The approach of defining three regions for heat transfer on the plate surface was addressed by Kutscher (1992) for an axisymmetric model (single slot). This approach was adopted in the present work and was applied for all existing slots (21) of the model.

The global effectiveness can then be expressed by:

$$\varepsilon_{UTC} = \varepsilon_f + \varepsilon_h + \varepsilon_b \tag{9}$$

Figure 7 and 8 show the three partial effectivenesses for the two plenum thicknesses and two mass fluxes (0.013 kg/s/m^2 and 0.0411 kg/s/m^2), respectively. Results are presented for an irradiance of 450 W/m^2 only.

As shown in Figure 7, the bulk of heat transfer occurs from the front face of the absorber plate and then from the slot. This observation is consistent with the results reported by (Abulkhair, 2011), and this is where the greatest temperature difference between the air and plate is experienced.

As the air mass flux increases through the UTC (Figure 8), the proportions of heat transfer on the front face and the slots decrease. This decrease is less important within the slots region, because the thermal boundary layer is not fully developed, and the dependence of the convection coefficient on the Reynolds number is low. Thus, the location at which most of the heat transfer is occurring moves more to the back-side of

the absorber plate with the air mass flux. This results in relatively large recirculating turbulent eddies at the slot outlet which spread on the surface of the back-side of the absorber plate. As a consequence, this results, in a better heat transfer effectiveness from the back-side. (Abulkhair, 2011) also reported a similar result.

Both Figure 7 and 8 show that the change in the plenum thickness does not have a large effect on the effectiveness distribution of the absorber plate (a difference of 0.7% is reported in Figure 7 for the back-side effectiveness while it is even lower at 0.5% in Figure 8).

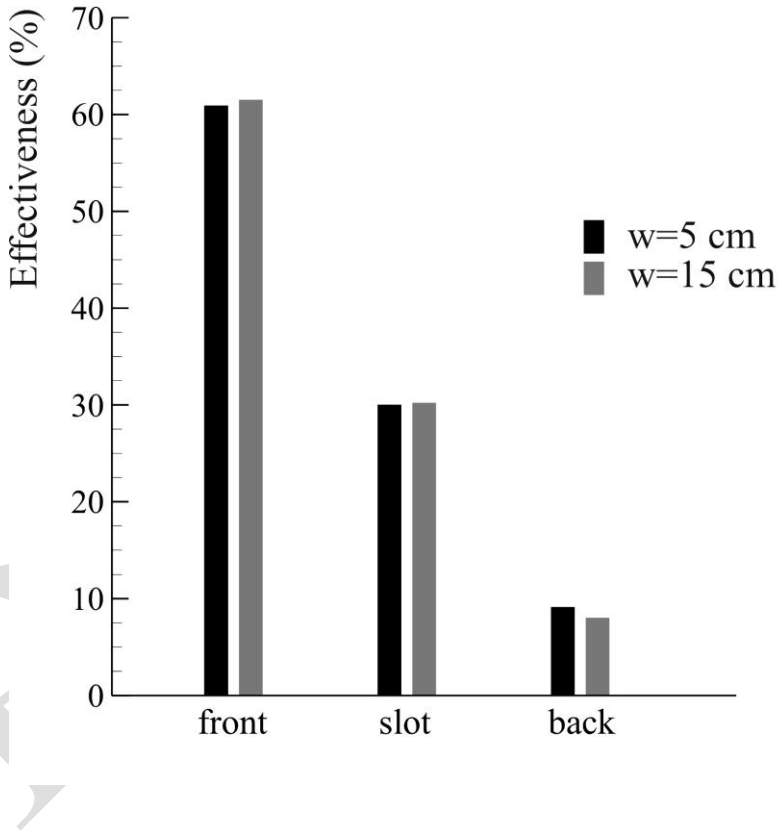

Figure 7: Heat transfer effectiveness occurring in the front, slot, and back of the-plate region for the two plenums cases with 0.013 kg/s/m^2

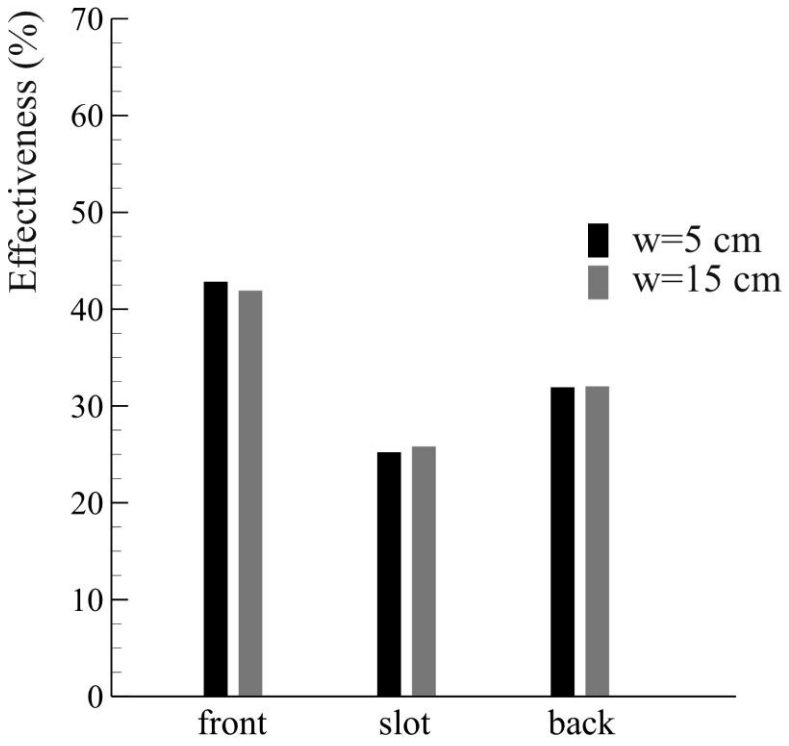

Figure 8: Heat transfer effectiveness occurring in the front, slot, and back of the-plate region for the two plenums cases with 0.0411 kg/s/m^2

6. Conclusion

The thermal efficiency of a UTC has been investigated both experimentally and numerically. Simulations and experiments were performed for two plenum thicknesses (w = 5 cm and 15 cm) at three air mass fluxes (0.0133, 0.0266, 0.0411 kg/s/m^2) and three irradiation levels (600, 450 and 300 W/m^2).

6.1. Research outcome (summary)

Results permit to conclude that:

- The efficiency increases with increasing air mass flux.
- The efficiency is relatively insensitive to the irradiance.

- The heat transfer is preponderant on the front (exposed) side of the absorber plate.
- The heat transfer preponderance moves progressively to the back-side of the absorber plate with increasing air mass flux.
- The efficiency of the collector and the effectiveness of the absorber plate are relatively insensitive to the plenum thickness.

6.2 Experiments and simulations

In all cases but one, simulations and experimental results were in good agreement within the experimental uncertainty.

For a low mass flux combined with a high irradiance, concordance was not excellent: the numerical predictions overestimated the measured efficiency by as much as 13% for the thickest plenum. This was discussed as due to the difficulty in the evaluation of the sky temperature required to compute the net radiant heat losses to the surroundings. This net heat loss increases with increasing irradiance and decreasing mass flux. Another source of discrepancy is the relative variation in the lab temperature (± 1.5°C) which mostly impairs the results for a low mass flux.

Nevertheless, this work provided sufficient confidence in the formulation and the implementation of the numerical procedure developed to predict and design UTCs.

6.3 Upcoming work

Several paths for the further developments of this work are now considered. First, a through parametric investigation of the problem with the numerical tool should be undertaken to extract more physical interpretation of the phenomena involved and confirm what has been observed herein. Second, a three-dimensional extension of the two-dimensional ideas implemented here should be carried out to grab the recirculation effects along the others axis and to considerer circular perforations instead of slots. Third, non-opaque surfaces (with variable transmissivities) should be considered as these are becoming more and more popular.

As a final remark, it is worth mentioning that there is a gap between laboratory and academic world, on the one hand, and industrial implementation, on the other hand. Both experimental and numerical work should be done in collaboration with practitioners of building refurbishment.

Acknowledgements

This work was supported by the t3e industrial research chair and its financial partners; the authors would like to acknowledge their invaluable contributions. The authors gratefully acknowledge the Centre de Technologies Thermiques (CTT) for research space.

References

Abulkhair, H, 2011. Thermal Analysis of Unglazed Transpired Solar Collectors. Universuty of Waterloo.

Arulanandam, SJ, et al., 1999. A CFD heat transfer analysis of the transpired solar collector under no-wind conditions. Solar Energy 67, 93-100.

Athienitis, AK, et al., 2011. A prototype photovoltaic/thermal system integrated with transpired collector. Solar Energy 85, 139-153.

Badache, M, et al., 2012. A full 3^4 factorial experimental design for efficiency optimization of an unglazed transpired solar collector prototype. Solar Energy 86, 2802-2810.

Badache, M, et al., 2010 Experimental characterization of an unglazed transpired solar collector. Proc. Eurosun, Graz, Austria.

Belusko, M, et al., 2008. Performance of jet impingement in unglazed air collectors. Solar Energy 82, 389-398.

Biona M, et al., 2002. Performance Curve Generation of an Unglazed Transpired Collector System for Solar Crop/Fish Drying. M. Sc. Thesis, De La Salle University, Manila.

Cao S, et al., 1993. Heat exchange effectiveness of unglazed transpired-plate solar collector in 2D flow. ISES Solar World Congress Budapest, Hungary, 351.

Celik, I, et al., 2008. Procedure for estimation and reporting of uncertainty due to discretization in CFD applications. ASME J. Fluids Eng 130.

Dymond, C, Kutscher, C, 1997. Development of a flow distribution and design model for transpired solar collectors. Solar Energy 60, 291-300.

Fleck, BA, et al., 2002. A field study of the wind effects on the performance of an unglazed transpired solar collector. Solar Energy 73, 209-216.

Fluent, 2012. User's Manual Guide, Version 12.1.4. Ansys Inc.

Fuliotto, R, et al., 2010. Experimental and numerical analysis of heat transfer and airflow on an interactive building facade. Energy and Buildings 42, 23-28.

Gawlik, K, et al., 2005. A Numerical and Experimental Investigation of Low-conductivity Unglazed, Transpired Solar Air Heaters. Journal of Solar Energy Engineering 127, 153-155.

Genevès, C, et al., 2012. Review of Unglazed Transpired Collectors (UTCs). Renewable & Sustainable Energy Reviews, (submited, sept 2012).

Gunnewiek, LH, et al., 1996. Flow distribution in unglazed transpired plate solar air heaters of large area. Solar Energy 58, 227-237.

Gunnewiek, LH, et al., 2002. Effect of wind on flow distribution in unglazed transpired-plate collectors. Solar Energy 72, 317-325.

Khattab, NM, 2001. Evaluation of perforated plate solar air heater. International Journal of Solar Energy 21, 45-62.

Kutscher, CF, 1994. Heat exchange effectiveness and pressure drop for air flow through perforated plates with and without crosswind. Journal Name: Journal of Heat Transfer, Series C); 116:2, 391-399.

Kutscher, CF, 1992. An investigation of heat transfer for air flow through low-porosity perforated plates. Ph.D. University of Colorado at Boulder, United States - Colorado.

Kutscher, CF, et al., 1993. Unglazed transpired solar collectors: heat loss theory. Journal of Solar Energy Engineering, Transactions of the ASME 115, 182-188.

Leon, MA, Kumar, S, 2007. Mathematical modeling and thermal performance analysis of unglazed transpired solar collectors. Solar Energy 81, 62-75.

Patankar, SV, Spalding, DB, 1972. A calculation procedure for heat, mass and momentum transfer in three-dimensional parabolic flows. International Journal of Heat and Mass Transfer 15, 1787-1806.

Quesada, G, et al., 2012a. A comprehensive review of solar facades. Opaque solar facades. Renewable and Sustainable Energy Reviews 16, 2820-2832.

Quesada, G, et al., 2012b. A comprehensive review of solar facades. Transparent and translucent solar facades. Renewable and Sustainable Energy Reviews 16, 2643-2651.

Rousse, D.R., 1994, Numerical predictions of multidimensional conduction, convection and radiation heat transfer in participating media, Ph.D. Thesis, McGill University, Canada.

Rousse, D.R., 1996, Numerical method for conduction, convection and radiation heat transfer in three-dimensional geometries, Proc. 2nd European Thermal-Sciences and 14th UIT National Heat Transfer Conference, Rome, 1425-1433.

Robert J, M, 1988. Describing the uncertainties in experimental results. Experimental Thermal and Fluid Science 1, 3-17.

Van Decker, GWE, et al., 2001. Heat-exchange relations for unglazed transpired solar collectors with circular holes on a square or triangular pitch. Solar Energy 71, 33-45.

Weerakoon, A, et al., 2004. Use of perforated metal sheets as solar collectors for building space heating. International Heat transfer Conference 132006. p. ENR-01.

Zhang, Z, et al., 2007. Evaluation of various turbulence models in predicting airflow and turbulence in enclosed environments by CFD: Part 2-Comparison with experimental data from literature. HVAC&R Research 13, 871-886